

SPIRITS: UNCOVERING UNUSUAL INFRARED TRANSIENTS WITH *SPITZER*

MANSI M. KASLIWAL¹, JOHN BALLY², FRANK MASCI³, ANN MARIE CODY⁴, HOWARD E. BOND^{7,10}, JACOB E. JENSON¹, SAMAPORN TINYANONT¹, YI CAO¹, CARLOS CONTRERAS⁵, DEVIN A. DYKHOFF⁶, SAMUEL AMODEO⁶, LEE ARMUS³, MARTHA BOYER^{8,22}, MATTEO CANTIELLO⁹, ROBERT L. CARLON⁶, ALEXANDER C. CASS⁶, DAVID COOK¹, DAVID T. CORGAN⁶, JOSEPH FAELLA⁶, ORI D. FOX¹⁰, WAYNE GREEN², ROBERT GEHRZ⁶, GEORGE HELOU³, ERIC HSIAO¹¹, JOEL JOHANSSON¹², RUBAB M. KHAN⁸, RYAN M. LAU^{1,20}, NORBERT LANGER¹³, EMILY LEVESQUE¹⁴, PETER MILNE¹⁵, SHAZRENE MOHAMED^{16,21,23}, NIDIA MORRELL⁵, ANDY MONSON⁷, ANNA MOORE¹, ERAN O. OFEK¹², DONAL O' SULLIVAN¹, MUDUMBA PARTHASARTHY¹⁷, ANDRES PEREZ¹, DANIEL A. PERLEY¹⁸, MARK PHILLIPS⁵, THOMAS A. PRINCE¹, DINESH SHENOY⁶, NATHAN SMITH¹⁵, JASON SURACE¹⁹, SCHUYLER D. VAN DYK³, PATRICIA WHITELOCK^{16,21}, ROBERT WILLIAMS¹⁰

¹Division of Physics, Mathematics and Astronomy, California Institute of Technology, Pasadena, CA 91125, USA

²Center for Astrophysics and Space Astronomy, University of Colorado, 389 UCB, Boulder, CO 80309, USA

³Infrared Processing and Analysis Center, California Institute of Technology, Pasadena, CA 91125, USA

⁴NASA Ames Research Center, Moffett Field, CA 94035, USA

⁵Las Campanas Observatory, Carnegie Observatories, Casilla 601, La Serena, Chile

⁶Minnesota Institute for Astrophysics, School of Physics and Astronomy, 116 Church Street, S. E., University of Minnesota, Minneapolis, MN 55455, USA

⁷Dept. of Astronomy & Astrophysics, Pennsylvania State University, University Park, PA 16802 USA

⁸NASA Goddard Space Flight Center, MC 665, 8800 Greenbelt Road, Greenbelt, MD 20771 USA

⁹Kavli Institute for Theoretical Physics, University of California, Santa Barbara, CA 93106, USA

¹⁰Space Telescope Science Institute, 3700 San Martin Dr., Baltimore, MD 21218 USA

¹¹Department of Physics, Florida State University, 77 Chieftain Way, Tallahassee, FL, 32306, USA

¹²Benozziyo Center for Astrophysics, Weizmann Institute of Science, 76100 Rehovot, Israel

¹³Argelander-Institut für Astronomie Auf dem Hgel 71. D-53121 Bonn, Germany

¹⁴Department of Astronomy, University of Washington Seattle, Box 351580, WA 98195-1580 USA

¹⁵Steward Observatory, University of Arizona, Tuscon, AZ 85721, USA

¹⁶SAAO, PO Box 9, Observatory, 7935, South Africa

¹⁷Indian Institute of Astrophysics, Koramangala, Bangalore 560034, India

¹⁸Dark Cosmology Centre, Niels Bohr Institute, Juliane Maries Vej 30, Copenhagen AF, DK-2100, Denmark

¹⁹Eureka Scientific, Inc. 2452 Delmer Street Suite 100 Oakland, CA 94602-3017 USA

²⁰Jet Propulsion Laboratory, California Institute of Technology, 4800 Oak Grove Drive, Pasadena, CA 91109, USA

²¹Astronomy Department, University of Cape Town, University of Cape Town, 7701, Rondebosch, South Africa

²²Department of Astronomy, University of Maryland, College Park, MD 20742 USA

²³National Institute for Theoretical Physics, Private Bag X1, Matieland, 7602, South Africa

ABSTRACT

We present an ongoing, systematic search for extragalactic infrared transients, dubbed SPIRITS — *SPitzer* InfraRed Intensive Transients Survey. In the first year, using *Spitzer*/IRAC, we searched 190 nearby galaxies with cadence baselines of one month and six months. We discovered over 1958 variables and 43 transients. Here, we describe the survey design and highlight 14 unusual infrared transients with no optical counterparts to deep limits, which we refer to as SPRITEs (eSPecially Red Intermediate Luminosity Transient Events). SPRITEs are in the infrared luminosity gap between novae and supernovae, with [4.5] absolute magnitudes between -11 and -14 (Vega-mag) and [3.6]-[4.5] colors between 0.3 mag and 1.6 mag. The photometric evolution of SPRITEs is diverse, ranging from <0.1 mag yr⁻¹ to >7 mag yr⁻¹. SPRITEs occur in star-forming galaxies. We present an in-depth study of one of them, SPIRITS 14ajc in Messier 83, which shows shock-excited molecular hydrogen emission. This shock may have been triggered by the dynamic decay of a non-hierarchical system of massive stars that led to either the formation of a binary or a proto-stellar merger.

Keywords: surveys, infrared, supernovae, AGB and post-AGB, novae, cataclysmic variables, mass-loss

1. INTRODUCTION

The systematic study of explosive transients and eruptive variables is growing by leaps and bounds especially with the

advent of wide-field synoptic imaging. Recently, multiple new classes of optical transients (e.g., Kasliwal 2012) and new radio transients (e.g., Thornton et al. 2013) have been uncovered. Yet, the dynamic infrared (IR) sky is hitherto largely unexplored.

While the optical is a powerful band to explore supernovae and novae, it is blind to transients and eruptive variables that are either self-obscured or located in dusty regions (e.g., molecular clouds). IR follow-up of optically discovered transients shows that IR emission dominates in supernovae with circumstellar interaction, particularly at late-time (Fox et al. 2011, 2013). We are now aware of at least two new classes of explosive transients where the bulk of the emission is in the IR – stellar mergers (associated with luminous red novae, e.g. V1309 Sco; Tylenda et al. 2011) and electron capture supernovae (eCSNe; associated with intermediate luminosity red transients, e.g. NGC300-OT; Bond et al. 2009, SN 2008S; Prieto et al. 2008).

Some efforts have been undertaken to look for IR transients and variables with the *Spitzer* Space Telescope (Werner et al. 2004; Gehrz et al. 2007). A blind search for IR transients in repeated imaging of the Bootes field revealed a superluminous supernova (Kozłowski et al. 2010). Searches targeting nearby star forming regions in the Milky Way have shown a plethora of young star variability (Cody et al. 2014; Rebull et al. 2014). Searches for variable, obscured asymptotic giant branch stars in nearby galaxies is being undertaken by the DUSTINGS survey (Boyer et al. 2015). Searches for obscured supernovae in starburst galaxies, using *Spitzer* (Fox et al. 2012), *HST* (Cresci et al. 2007) and high-resolution ground-based adaptive optics imaging (e.g., Mattila et al. 2007), have revealed a few candidates (Kankare et al. 2008, 2012).

Motivated thus, we began a systematic search for mid-IR transients in nearby galaxies with *Spitzer*. Here, we present the experiment design (§2), the software pipelines (§3), the discoveries in the first year (§4) and a case-study (§5). We conclude with reflections on a possible way forward to chart the dynamic IR sky (§6).

2. EXPERIMENT DESIGN

2.1. Galaxy Sample, Cadence and Depth

The SPIRITS experiment uses the IRAC instrument (FoV $5' \times 5'$; Fazio et al. 2004) aboard the warm *Spitzer* telescope to search for IR transients at $3.6 \mu\text{m}$ ([3.6]) and $4.5 \mu\text{m}$ ([4.5]). This is a search targeting 190 nearby galaxies selected using three criteria: (i) 37 galaxies out to 5 Mpc spanning diverse galaxy environments: early-type galaxies, late-type galaxies, dwarf galaxies and giant galaxies (ii) 116 luminous galaxies between 5 Mpc and 15 Mpc. Our sample of galaxies captures a total of $2.0 \times 10^{12} L_{\odot}$ in the B-band within 15 Mpc. This is 83% of the total B-band starlight within the < 15 Mpc volume. (iii) The 37 most luminous and most massive galaxies in the Virgo Cluster (17 Mpc). These galaxies total $1.6 \times 10^{12} L_{\odot}$

i.e. 66% of the total B-band luminosity of the cluster. Furthermore, these galaxies total $9.1 \times 10^{11} M_{\odot}$ i.e. 71% of the total stellar mass of the cluster.

Tables summarizing properties of galaxies in this sample in detail is presented in Kasliwal et al. 2013. In 2015 and 2016, we added star-forming regions in galaxies too large to map with IRAC otherwise (Kasliwal et al. 2014a). In 2017 and 2018, we down-sized the sample to focus on the most luminous and most massive galaxies (Kasliwal et al. 2016).

In 2014, each of these galaxies was imaged three times by SPIRITS, with cadence baselines of 1 month and 6 months. In 2015 and 2016, additional shorter cadence baselines of 1 week and 3 weeks were added. Archival data provides us additional multi-year baselines. A histogram of cadence baselines is available in Kasliwal et al. 2014a.

Each SPIRITS pointing is seven dithered 100 s exposures in each IRAC filter. The limiting magnitude (as defined for a 5σ point source Vega magnitude) in each SPIRITS epoch is 20 mag at [3.6] and 19.1 mag at [4.5]. This gives us a [3.6] depth of up to -8.5 mag at 5 Mpc and up to -11.5 mag at 20 Mpc.

2.2. Follow-Up Ground-based observations

We are undertaking concomitant ground-based surveys to monitor the SPIRITS galaxy sample in the near-IR and the optical at roughly a monthly cadence. At the University of Minnesota’s Mt Lemmon Observing Facility (MLOF), we use the three-channel Two Micron All Sky Survey cameras (Milligan et al. 1996; Skrutskie et al. 2006) mounted on the 1.52m IR telescope (Low et al. 2007). At Las Campanas, we undertake near-IR monitoring with the Retrocam on Dupont 100-inch telescope and optical monitoring using the CCD on the Swope 40-inch telescope. At Palomar, we use the Samuel Oschin 48-inch (primarily *r*-band) and Palomar 60-inch telescopes (*gr*-bands) for optical monitoring. Using the LCOGT network, we obtain additional optical monitoring in *gi*-bands. In addition, follow-up of discovered transients was undertaken by a myriad of facilities including Keck, Magellan, Palomar 200-inch, SALT and RATIR.

2.3. Follow-Up with the Hubble Space Telescope

Following non-detections from the ground, we were able to set even deeper magnitude limits for two transients based on a small *HST* Director’s Discretionary program (GO/DD-13935, PI H. Bond). We imaged SPIRITS 14aje (in M101) and SPIRITS 14axa (in M81) with the Wide Field Camera 3 (WFC3) in 2014 September. In the WFC3 UVIS channel, we employed an “*I*” filter (F814W), and in the IR channel we used “*J*” (F110W) and “*H*” (F160W) bandpasses. The sites of both targets had been observed with *HST* before their outbursts, making it possible for us to compare our new images with the archival data. We registered the *Spitzer* frames with the *HST* frames by measuring the positions of isolated stars detected in both images, allowing the sites of the transients to

be located in the *HST* images to precisions of typically $0''.1$ (More details in Bond et al. in prep).

3. SOFTWARE PIPELINES

3.1. Image Subtraction and Source Catalogs

We construct reference images using archival *Spitzer* imaging using supermosaics or S4G stacks (Sheth et al. 2010; where supermosaics were unavailable) or stacking prior “bcd” observations in the archive (where neither supermosaics nor S4G stacks were available). We use the “maic” products of the *Spitzer* IRAC pipeline as our starting point for difference imaging. We adapted an image differencing and transient-source extraction code developed for the Palomar Transient Factory (PTFIDE¹) to *Spitzer* imaging. The changes made to this software were (i) ability to operate on co-adds of individual IRAC exposures; (ii) masking of co-add-image regions with depths <5 exposures to mitigate cosmic rays and detector glitches; (iii) execution of the SExtractor tool (Bertin and Arnouts, 1996) to extract transient candidates from the difference images (as opposed to PSF-fitting for PTF); (iv) omission of dynamic photometric-gain matching between reference and science-image co-adds, and (v) a more streamlined and simpler PSF-matching scheme between images. Updates (iv) and (v) take advantage of the stable thermal environment of the *Spitzer* telescope. Examples of discovery image triplets are shown in Figure 1.

One may expect difference-imaging from space to yield fewer false positives than from a ground observatory where atmospheric conditions continuously modify the PSF between observations, however, we found this generally not to be the case with *Spitzer* (in part, due to the sparsely sampled PSF). The *Spitzer* difference-imaging is prone to a large number of false positives when the *Spitzer* field-of-view had a large rotation between the reference and science image epochs. The *Spitzer*-IRAC PSF profiles follow the fixed detector/optical diffraction patterns and these could not be easily matched and subtracted between rotated apparitions of the same piece of sky. Each of our candidates are visually vetted and we require at least two detections (in two filters or at two epochs) to weed out false positives. But, we caution that our search is incomplete and any inferred rates of transients are likely lower limits.

3.2. Forced Photometry

We define a source to be transient if there is no detected quiescent point source underneath the source location in the reference frame (else, the source is a variable). To obtain magnitudes for transient sources, we perform forced aperture photometry on the subtracted images, assuming zero flux present in the reference image. We sum the flux in an aperture with radius 4-pixels ($2''.4$) centered at the RA and Dec coordinates

determined by our transient detection routines. Sky background is measured within an annulus from 8 to 16 pixels surrounding each source and subtracted from the total flux. Finally, fluxes are converted to magnitudes using the Warm *Spitzer*/IRAC zero points of 18.8024 (channel 1) and 18.3174 (channel 2), along with aperture corrections of 1.21 and 1.22, respectively, as specified by the IRAC instrument handbook. Since the subtraction images are noisy, we conservatively set the detection and upper limit threshold at 9σ .

3.3. Database and Dynamic Web Portal

We architected a postgresql database to ingest the difference imaging products. The search for transients is undertaken via a dynamic web portal. In 2014, *Spitzer* data was released every two weeks (the time-lag has now been reduced to only a few days). Once the data is released, the SIDE pipeline is promptly run. Team members are assigned galaxies to look through candidate metadata and postage stamps to visually vet and flag interesting transients, typically within one day of data release. These transients are then assigned a name in sequential order by the database. For example, in the first year, a total of 131722 candidates (on 4396 new and archival subtraction images) were automatically loaded into our subtraction database. Of these, only 1693 sources were assigned names and flagged for further inspection as transients or variable stars. Additional context information from various ground-based and space-based facilities is summarized on a source-specific webpage for reference. Interesting transients are announced via Astronomers Telegrams (e.g., Kasliwal et al. 2014b; Jencson et al. 2015, 2016a,b).

4. FIRST TRANSIENT DISCOVERIES

In the first year, SPIRITS detected over 1958 variable stars and 43 IR transient sources. Of these 43 transients, 21 were known supernovae and 4 were in the luminosity range of classical novae. SPIRITS supernovae have been discussed in-depth as a Type Ia sample (Johansson et al. 2014), a core-collapse sample (Tinyanont et al. 2016), and a case-study of the peculiar low-velocity SN 2014dt (Fox et al. 2016). Four transients had optical counterparts: SPIRITS 14axm in NGC 2403 (luminous blue variable; van Dyk et al. in prep), SPIRITS 14pz in NGC 4490 (stellar merger candidate; Smith et al. 2016), SPIRITS 14bme in NGC 300 (high mass X-ray binary; Lau et al. 2016) and SPIRITS 14bmc in NGC 300 (Adams et al. in prep). Here, we discuss the remaining 14 events (see Table 1), which are unusual IR transients in the luminosity gap between novae and supernovae with no optical counterparts, hereafter referred to as SPRITEs (eSPecially Red Intermediate-luminosity Transient Events).

The common properties of this new class of SPRITEs are:

1. Peak luminosity at [4.5] brighter than -11 mag and fainter than -14 mag (see Table 2).
2. IRAC Color [3.6]-[4.5] between 0.3 mag and 1.6 mag

¹ <http://web.ipac.caltech.edu/staff/fmasci/home/miscscience/ptfide-v4.0.pdf>

(see Table 2).

3. No optical counterpart in concomitant or follow-up imaging to at least $r < 20$ mag (see Table 4).
4. Occurring in star-forming galaxies even though the SPIRITS galaxy sample has a mix of all galaxy types (see Figure 2)

First, we place SPRITEs in context of the IR transient phase space. We plot the IR luminosity evolution of SPRITEs and compare to well-known novae and supernovae (see top panel of Figure 3). SPRITEs are too luminous to be classical novae. The highest absolute magnitude that can be achieved by dusty classical novae is approximately -11 mag at [3.6]. This maximum occurs when an optically thick dust shell forms about 50–100 days after outburst while the central engine is still near Eddington luminosity (e.g. NQ Vul, LW Ser; see Gehrz et al. 1995). At peak dust production, these novae can have a [3.6]-[4.5] color of ≈ 1.5 mag (see Ney & Hatfield 1978; Gehrz et al. 1980). Some very fast novae that do not form dust (e.g. V1500 Cyg; see Gallagher & Ney 1976; Ennis et al. 1977) may also reach luminosities of up to ≈ -11 mag for a few days at outburst.

Next, we characterize the light curves of SPRITEs. The *Spitzer* light curve data are presented in Table 5. We broadly categorize SPRITEs into two relative speed classes (see Table 2): (i) six SPRITEs evolve slowly over many year timescales with speeds slower than 0.5 mag yr^{-1} (Figure 6), (ii) eight SPRITEs evolve faster than 0.5 mag yr^{-1} (Figure 4). Of these, four evolve on few month timescales, faster than 1.5 mag yr^{-1} and fade below detectability in less than one year.

But, the light curve comparison is limited as the light curves of SPRITEs are diverse, infrequently sampled and the explosion times are poorly constrained. Therefore, we plot IR luminosity versus IR color at all epochs (bottom panel of Figure 3). We find that SPRITEs occupy a unique region in phase space between novae and supernovae on this dynamic HR diagram of explosive IR transients. We note that the IR colors of SPRITEs are as red as the reddest novae, core-collapse supernovae and ILRTs. The corresponding effective black body temperatures of SPRITEs span 350 K to 1000 K.

The puzzling absence of optical emission from SPRITEs challenges a supernova interpretation. Typical supernovae are brighter than 20 mag at 20 Mpc for many months in the visual wavebands. Thus, no prior history of optical detection (despite the intensive monitoring of nearby galaxies by several synoptic surveys and amateurs in the optical wavebands) suggests that SPRITEs are unlikely to be old supernovae. If the IR explosion time is strongly constrained and the lifetime is shorter than a year, it implies that the peak luminosity was not much higher than observed (and, that the transient is not old). We consider the hypothesis that two fast SPRITEs — SPIRITS 14axa and SPIRITS 14bay — are obscured supernovae. Applying a simple extinction law to a 10,000 K black-

body (Cardelli et al. 1989; Chapman et al. 2009), we find that an observed [3.6]-[4.5] color of 1 mag requires visual extinction of 30 mag respectively! This is difficult especially given the location of SPRITEs in the middle-to-outer galaxy disks (Figure 2). Moreover, if this is correct, given that there were six new optical supernovae in the SPIRITS sample in 2014, it would suggest that optical surveys are missing a fourth of the supernovae due to obscuration.

Next, there are a few possible theoretical models that may explain SPRITEs. For example, coalescence of 1–30 M_{\odot} binaries is expected to create copious amounts of dust in an optically thick wind launched during the stellar merger (Soker & Tylenda 2006; Ivanova et al. 2013; Nicholls et al. 2013; Pejcha et al. 2016). Another possibility is that these are electron-capture induced collapse of 8–10 M_{\odot} extreme AGB stars where the shock breakout did not destroy all the dust surrounding the progenitor (Kochanek 2011). Yet another possibility is that weak shocks in failed supernovae that form black holes may also not lead to bright optical transients but rather IR transients as the ejection of large amounts of material at low velocity may condense to form dust (Piro 2013; Lovegrove & Woosley 2013). We consider the likelihood of each of these models below.

The speed of evolution is diagnostic of the origin in that a terminal, explosive event (eCSNe, obscured SNe, failed SNe) would likely belong to the fast class and a stellar merger would likely belong to the slow class. Stellar merger of massive stars may result in a slowly evolving red remnant. As was seen with SPIRITS 14pz in NGC 4490 (Smith et al. 2016) and the transient in M 101 (Blagorodnova et al. 2016), the SPRITE luminosities are consistent with late-time observations of a stellar merger. The young stellar population in the vicinity of these transients also supports the presence of massive stars. Five slow SPRITEs could be stellar mergers (We exclude SPIRITS 14bgq as it repeats – appears, disappears and re-appears – and could either be a background AGN or an extreme AGB variable). If this hypothesis is correct, the rates appear to be higher than that estimated by Kochanek et al. 2014.

Now for the relatively fast events, the nature of the explosion can be disentangled if there is a progenitor identification. Distinguishing features of the eCSNe class are: (i) the detection of an IR progenitor star with an absolute magnitude brighter than -10 mag and color redder than 1 mag (Thompson et al. 2009; Kochanek 2011), and (ii) subsequently, a monotonic decline of the transient emission below the progenitor luminosity (Adams et al. 2016). Only two SPRITEs have detections in archival *Spitzer* imaging: SPIRITS 14bgq and SPIRITS 14bsb. But neither is a promising eCSN as SPIRITS 14bgq is eruptive (not explosive) and SPIRITS 14bsb appears to be part of a massive star cluster. The remaining SPRITEs have upper limits deep enough (see Table 2) to rule out most of the progenitor parameter space delineated by Thompson et al. 2009.

If an HST progenitor is detected and consistent with a massive star, there are two possibilities: an eruption event like eta Carinae or a terminal explosive event like the formation of a stellar mass black hole. Both would be consistent with a young population. One way to distinguish these two would be to continue monitoring to see if the fading is monotonic (hence, terminal) or if there is another episode of eruption. But none of the SPRITEs with both pre-explosion and post-explosion archival HST imaging have candidate progenitor counterparts. Specifically, our HST imaging of SPIRITS 14aje in 2014 September shows only one faint star detected at the edge of a 3σ positional error circle in *I*-band. But this star does not vary between 2003 and 2014, is not detected in the *J*-band and *H*-band and likely unrelated to the transient. Similarly, our HST imaging in *I*-band of SPIRITS 14axa shows one star that brightened by ~ 0.4 mag between 2002 and 2014, but it is consistent with a normal field red giant lying close to the tip of the red-giant branch and likely unrelated.

In summary, the IR photometric data alone is not sufficient to distinguish between various models. Ground-based spectroscopic data has been difficult to obtain because these transients are either very faint or not detected in the near-IR/optical wavelengths. Next, we present a detailed case-study on one transient for which we see shock-excited emission lines in a near-IR spectrum and hence, infer a physical origin.

5. SPIRITS 14AJC: A TRANSIENT DRIVING A SHOCK INTO A MOLECULAR CLOUD

SPIRITS 14ajc in M 83 went into outburst in 2010 and has stayed at a [3.6]-band luminosity of -11 mag and a [3.6]–[4.5] color of 0.7 mag for the past four years (Figure 6). No quiescent source was detected in *Spitzer* images taken between 2006 and 2008. No optical or near-IR counterpart is detected in ground-based follow-up in 2014 (see Table 4). Based on the cool SED of the transient, the effective blackbody temperature is approximately 900 K.

SPIRITS 14ajc is located in a spiral arm of M 83 with intense star formation (Figure 2). The 2.6 mm ^{12}CO J=1–0 emission at the position of SPIRITS 14ajc, measured with the Nobeyama Millimeter Array (Hirota et al. 2014), has a peak brightness temperature of 2.8 K, a velocity integrated flux $I(\text{CO}) = 28.6$ Kelvin km s $^{-1}$ in the 6'' by 12'' synthesized beam, and is centered at $V_{\text{LSR}} = 572 \pm 15$ km s $^{-1}$. The X-factor method (Bolatto et al. 2013) to convert $I(\text{CO})$ into H $_2$ column density using a Solar-vicinity value for the X-factor (2.0×10^{20} cm $^{-2}$ K $^{-1}$) gives $N(\text{H}_2) \approx 5.7 \times 10^{21}$ cm $^{-2}$ per beam corresponding to a visual-wavelength (V-band) extinction of 6 mag if the cloud were distributed uniformly over the beam. The NMA beam-size corresponds to a physical scale of 128 pc \times 279 pc at the distance of M 83, making it likely that the extinction is patchy and potentially higher along the line of sight to SPIRITS 14ajc.

A *K*-band spectrum obtained with the MOSFIRE spectrometer (McLean et al. 2012) on the Keck I 10-meter telescope on 8 June 2014 found five emission lines of molecular hydrogen, and neither any continuum nor any other lines. The observed properties of these ro-vibrational transitions are summarized in Table 3. The velocities are consistent with the CO radial velocity at the position of SPIRITS 14ajc. The relative line intensities of the four $v=1-0$ ro-vibrational transitions are consistent with shock-excitation at a temperature around 1000 to 2,000 K and similar to the relative intensities in Herbig-Haro objects such as HH 211 (O’Connell et al. 2005). However, the intensity ratio of the $v=2-1$ to $1-0$ vibrational transition corresponds to a higher temperature, possibly indicating that fluorescent pumping in the ultraviolet Lyman and Werner bands may play a role in exciting the higher vibrational states of H $_2$, or that the shock structure in the emission regions has a more complex temperature structure.

The site of SPIRITS 14ajc in M83 was fortuitously imaged by *HST* with the WFC3 camera in 2012 (program GO-12513, PI W. Blair). The SPIRITS 14ajc light curve suggests that the event was underway in 2012, although unfortunately there were no *Spitzer* observations in this year. Figure 6 depicts the site of SPIRITS 14ajc in the *HST* *V*, *I*, H α + $[\text{N II}]$, and *H* bandpasses. The source lies in a very crowded stellar field with only modest extinction. In the *I*-filter, there is a faint star (26.0 mag, $M_I \simeq -3.8$) which lies close to the center of the error circle and a brighter star (25.0 mag, $M_I \simeq -2.8$) which lies at the eastern edge of the 3σ position uncertainty. The absolute magnitudes are consistent with both stars being normal field red giants. Only the brighter of these two stars is marginally detected at *V* and neither star is detected in *H*-band. In the absence of any other *HST* images in these filters taken at different dates, we cannot definitely rule out that either of the *I*-band sources is the counterpart of SPIRITS 14ajc, but the lack of a detection at *H* argues against this. The 5σ limiting magnitude (Vega-scale) for the *H*-band exposure is about 23.5. The H α + $[\text{N II}]$ image (third frame) shows nothing at the site, but nearby is a small, faint, bubble-like emission nebula just outside the error circle. Its diameter is about 0''.6, or approximately 16 pc. To characterize the stellar and ISM environment, we show a color rendition of its wider surroundings. There are several young associations, some containing red supergiants, as well as a network of dark dust lanes, within a few arcseconds of the site. However, 14ajc is not clearly associated with either the very young clusters or dark dust features.

We consider two models for SPIRITS 14ajc: the explosion of a supernova immediately behind or inside a dense molecular cloud (Kasliwal et al. 2005), and the production of an eruptive protostellar outflow similar to the explosion that occurred in Orion about 500 years ago (Zapata et al. 2009; Bally et al. 2011, 2015).

5.1. Is SPIRITS 14ajc powered by a supernova?

In the supernova scenario, two mechanisms may contribute to the IR signal. First, the flash produced by the explosion can be reprocessed into the IR portion of the spectrum by dust as the light echo propagates through the dense interstellar medium. In this scenario, foreground dust completely extinguishes the visual to near-IR wavelength signature of the event. Second, if the supernova is sufficiently close to a dense cloud, the impact of the forward shock can excite H₂ emission as the blast-wave slams into a dense molecular medium. There may be two components to this emission: collisional excitation of H₂ in the swept-up, compressed, and accelerated, post-shock layer, and fluorescent excitation by the UV radiation emitted by fast shocks. Shock radiation can excite both H₂ located ahead of the shock, and surviving or reformed H₂ in the swept-up, post shock layer. A visual extinction of more than 15 mag is required to hide the visual and near-IR continuum of a supernova.

The ionizing radiation of the supernova progenitor should have created a large ionized cavity in the surrounding ISM. However, there is no obvious HII region at the location of SPIRITS 14ajc. It is possible that foreground dust obscures any cavity or HII region. Alternatively, a high-velocity, ‘runaway’ OB-star would have only carved a small cavity. More than 30% of massive OB stars are ejected from their birth sites with velocities greater than 20 km s⁻¹, and more than 10% with velocities larger than 100 km s⁻¹ (Gies & Bolton 1986). Two ejection mechanisms have been identified: dynamical interactions such as the re-arrangement of the non-hierarchical multiple stars into a hierarchical configuration such as a compact binary and ejected members. (Hoogerwerf et al. 2000, 2001; Gualandris et al. 2004), and the supernova explosion of the most massive member of an OB-star binary which results in the ejection of the surviving member at its pre-supernova Keplerian orbital speed. Alternatively, if the runaway O star were in a red-supergiant phase prior to its demise as a supernova as it entered a molecular cloud, it would have avoided the production of an ionized cavity. It is also possible that the supernova was a Type Ia which happened to drift into a molecular cloud. However, such events must be rare since the volume filling factor of dense molecular clouds in a galaxy tends to be less than 1%.

5.2. *Is SPIRITS 14ajc powered by a massive protostellar eruption?*

In the second model, the SPIRITS 14ajc transient may trace an explosion triggered by either a protostellar collision or a violent dynamical interaction of several massive protostars (Davies et al. 2006; Dale & Davies 2006). Such an event is suggested to have occurred in the OMC1 cloud core in the Orion A molecular cloud located behind the Orion Nebula, the nearest region of ongoing massive star formation ($D \approx 414$ pc; Menten et al. 2007). The OMC1 outflow consists of a spectacular, wide opening-angle, arcminute-scale (0.1 to 0.3 pc) outflow which is the brightest source of near-IR H₂ emission

in the sky (Allen & Burton 1993; Kaifu et al. 2000; Zapata et al. 2009; Bally et al. 2011, 2015). The radial velocity of the brightest part of the H₂ emission exhibits a line-width of less than about 70 km s⁻¹, consistent with the H₂ line-widths of SPIRITS 14ajc. Radial velocities and proper motions of more than 300 km s⁻¹ are observed in visual and near-IR spectral lines such as [OI], [SII], and [FeII]. The momentum and kinetic energy is at least 160 M_⊙ km s⁻¹ and 4×10^{46} ergs (Snell et al. 1984) to 4×10^{47} ergs (Kwan & Scoville 1976). Zapata et al. (2009) presented a CO J = 2–1 interferometric study and found a dynamic age of about 500 years for the larger OMC1 outflow. The initial explosion energy required to drive the observed outflow is between 10⁴⁷ to 10⁴⁸ ergs.

High-velocity, runaway stars are common among massive stars (Hoogerwerf et al. 2000; Gualandris et al. 2004). Radio-frequency astrometry has shown that two radio-emitting stars in OMC1, the 10 to 15 M_⊙ Becklin-Neugebauer (BN) object, and radio source I, thought to have a mass of about 20 M_⊙ (Goddi et al. 2011), have proper motions of 25 and 14 km s⁻¹ respectively away from a region less than 500 AU in diameter from which they were ejected about 500 years ago (Rodríguez et al. 2005; Gómez et al. 2008; Goddi et al. 2011). The kinetic energy in stellar motions is about 4×10^{47} ergs. The total energy of the OMC1 event, $\sim 10^{48}$ ergs, consists of the kinetic energy in the ejected stars, the current kinetic energy of the outflow, and the energy radiated away by shocks over the last 500 years (Bally et al. 2011).

Bally & Zinnecker (2005) proposed that the OMC1 explosion was triggered by the collision and merging of forming massive stars. Dynamic friction and Bondi-Hoyle accretion onto massive protostellar core inside a dense cluster-forming clump may have lead to rapid migration of the most massive protostars to the center of the clump’s potential well where they formed a non-hierarchical system of massive stars with similar interstellar separations. Such systems are unstable; interactions led to the formation of a hierarchical system consisting of a compact binary and a distant third member ~ 500 years ago. In this scenario, the final 3-body encounter would have resulted in the formation of a compact, AU-scale binary, most likely source I, and the ejection of both radio source I and BN from the OMC1 core Bally et al. (2011).

Goddi et al. 2011 used N-body simulations to show that the most likely initial configuration of massive stars in OMC1 that led to the observed current configuration of ejected stars consists of a massive binary star interacting with another massive star. The interaction leads to a hardening of the binary and consequent release of gravitational potential energy.

Binary stars are common among massive stars and the mass distribution is peaked at similar component masses. A massive binary can form from the bar instability in a massive disk. This mechanism tends to produce circular orbits in the plane of circumbinary and/or circumstellar disks. In forming clusters with a high density of protostars, massive stars surrounded by massive disks also have a high probability of capturing

clusters members to form binaries (Moeckel & Bally 2006, 2007b). The secondary in such a capture-formed binary is most likely to be on a high-eccentricity, high-inclination orbit with respect to the spin axis of the massive stars and its disk (Moeckel & Bally 2007a; Cunningham et al. 2009). Thus, binary-binary or binary-single star interactions are likely in dense proto-clusters.

The kinetic energy of the outflow and ejected stars came from the release of gravitational binding energy of a compact binary formed by the interaction of three or more stars. The total energy liberated by the formation or hardening of a binary depends on the stellar masses, M_1 and M_2 , and the orbit semi-major axis, R , as $E_B \approx GM_1M_2/2R$. For stars in the mass range 10 to 100 M_\odot and binary separation $0.5 < R < 10$ AU E_B ranges from 10^{47} to 10^{51} ergs. Assuming that radio source I consists of a pair of 10 M_\odot stars and that the energy required to eject the stars, the outflow, and to account for radiative losses is $E = 10^{48}$ ergs, the semi-major axis of the final binary must be $R \sim GM^2/2E \approx 0.9$ AU.

Forming massive stars accreting at rates of $\sim 10^{-4}$ to $\sim 10^{-3} M_\odot \text{ yr}^{-1}$ tend to have bloated, AU-scale photospheres and resemble red supergiants (Hosokawa & Omukai 2009). Radio source I has a photospheric temperature of ~ 4000 K, consistent with high-accretion models (Testi et al. 2010). If at least one star before the interaction were accreting at such a high rate, the 10^{48} erg energy requirement of the OMC1 event implies that any attempt to form an AU-scale binary would have led to a protostellar collision and consequent ejection of some of the bloated star’s photosphere before ejection from the cloud core.

In the dynamical interaction model, the disruption of circumstellar disks by the final close-in 3-body stellar encounter, combined with the recoil of the larger-scale envelope power the OMC1 outflow and a luminous IR flare. Ejected material slams into the surrounding cloud core and lower-density envelope with speeds comparable to the Kepler speed at their point of origin. Ejecta velocities are expected to range from 10s of km s^{-1} for material originating tens of AU to over 500 km s^{-1} for ejecta from within a few tenths of an AU of a massive star. The X-ray, UV, and visual light from shocks will be obscured and reprocessed by the surrounding cloud into the IR. Powerful shocks can produce an IR flare with luminosities up to 10^{51} ergs for the most massive star collisions (Bally & Zinnecker 2005).

The duration of the IR-flare is given by the shock crossing time of the part of the clump sufficiently dense to reprocess the shock-energy into the IR. The kinetic energy of the outflow is converted by surrounding dust to the mid and far-IR where the clump density is sufficiently large. Taking a clump radius, $R_{\text{clump}} \sim 0.01 - 0.05$ pc and an initial ejecta velocity of $V_{\text{ejecta}} \sim 500 \text{ km s}^{-1}$ implies a crossing time $t_{\text{cross}} \sim R_{\text{clump}}/V_{\text{ejecta}} \sim 20$ to 100 years. Emission of 2×10^{47} ergs in 20 years, a lower bound on the early radiative losses for an Orion-like event, implies a mean luminosity of

$10^5 L_\odot$.

The Orion OMC1 explosion is not unique among star forming regions. Zapata et al. (2013) found evidence for a powerful explosive outflow in the DR 21 complex in Cygnus. If such dynamic interactions are responsible for the large number of runaway O stars, and binaries among massive stars, the event rate of OMC1-like events ought to be comparable to the birth-rate of massive stars. We propose that SPIRITS 14ajc may trace the IR flare produced by a dynamic interaction of forming massive stars that either led to the formation of or hardening of a compact, AU-scale binary, or possibly a proto-stellar merger.

6. CONCLUSION AND A WAY FORWARD

SPIRITS has discovered a class of unusual IR transients called SPRITEs. SPRITEs are in the luminosity gap between novae and supernovae, with mid-IR [4.5] absolute magnitudes between -11 to -14 mag (Vega) and [3.6]-[4.5] colors between 0.3 mag and 1.6 mag. The photometric evolution of SPRITEs is diverse, ranging from $<0.1 \text{ mag yr}^{-1}$ to $>7 \text{ mag yr}^{-1}$. SPRITEs appear to represent diverse physical origins and each one merits an in-depth investigation to decipher its nature. Next, we address challenges encountered in the first year of the SPIRITS survey and efforts to overcome them.

A challenge in deciphering the nature of SPRITEs was the sparse sampling of their mid-IR light curves (due to the small number of epochs) with poor constraints on their explosion date (relative to archival images taken many years ago). Subsequent transients discovered in later years of the SPIRITS survey have both a better cadence on their light curve (1 week and 3 week cadence baselines were added) and better constraints on their explosion date (as the 2014 SPIRITS data serve as a reference).

Another challenge in the first year was the difficulty of immediate ground-based follow-up due to the delay of availability of *Spitzer* data and the mismatch between *Spitzer* and ground-based visibility. Both of these have improved in later years with *Spitzer* introducing early data release for time-critical programs and the additional SPIRITS cadence baselines being scheduled preferentially in time windows that facilitate ground-based follow-up.

Yet another challenge was identifying possible progenitor stars due to a combination of a dense stellar population in these nearby galaxies and the coarse *Spitzer* resolution. In order to address this, we now have an ongoing Hubble Space Telescope program to image these IR transients while they are still active.

Our study of SPIRITS 14ajc highlights the importance of spectroscopy in solving the mystery of the physical nature of the transient. Specifically, detecting the excited molecular hydrogen lines pointed to a shock driven by the dynamical decay of a non-hierarchical system of massive stars. However, spectroscopy has also been extremely challenging as these transients are too red for ground-based instruments, *Spitzer* is too

warm now for mid-IR spectroscopy and SOFIA is not sensitive enough for these faint transients. Spectroscopy with the James Webb Space Telescope (JWST) of slowly evolving SPIRITS transients would shed light on their nature. Specifically, the low resolution spectrometer could determine dust mass, grain chemistry, ice abundance and energetics to disentangle the proposed origins.

Regardless of the open questions on their origin, the discovery of SPRITEs representing a new class(es) of IR transients at a rate comparable (or higher) than supernovae is encouraging and motivates a synoptic IR search. However, undertaking a wide-field IR search for transients beyond targeting nearby galaxies requires overcoming the formidable challenge posed by the night sky brightness and detector cost. Concepts with alternative semiconductors (Sullivan et al. 2014) or creative optics on polar sites (Moore et al. in prep) are being investigated. If WFIRST elects a suitable survey design and prioritizes near real-time transient identification, it could be a powerful probe to discover IR transients.

In summary, the SPIRITS discovery of SPRITEs bodes well for future wide-field explorations of the dynamic IR sky.

We thank O. Pejcha, E. Lovegrove, S. Woosley, A. L. Piro, E. S. Phinney, S. R. Kulkarni, L. Bildsten and E. Quataert for valuable discussions. This work is based on observations made with the Spitzer Space Telescope, which is operated by the Jet Propulsion Laboratory, California Institute of Technology under a contract with NASA. The SPIRITS team acknowledges generous support from the NASA *Spitzer* grants for SPIRITS. MMK thanks the National Science Foundation for a PIRE Grant No. 1545949 for the GROWTH project. JJ acknowledges the National Science Foundation Graduate Research Fellowship under Grant No. DGE-1144469. PAW and SM are grateful to the South African National Research Foundation (NRF) for a research grant. RDG and the MLOF group were supported, in part, by the United States Air Force.

REFERENCES

- Adams, S. M., Kochanek, C. S., Prieto, J. L., Dai, X., Shappee, B. J., & Stanek, K. Z. 2016, *MNRAS*, 460, 1645
- Allen, D. A., & Burton, M. G. 1993, *Nature*, 363, 54
- Bally, J., Cunningham, N. J., Moeckel, N., Burton, M. G., Smith, N., Frank, A., & Nordlund, A. 2011, *ApJ*, 727, 113
- Bally, J., Ginsburg, A., Silvia, D., & Youngblood, A. 2015, *A&A*, 579, A130
- Bally, J., & Zinnecker, H. 2005, *AJ*, 129, 2281
- Blagorodnova, N., Kotak, R., Polshaw, J., et al. 2016, arXiv:1607.08248
- Bolatto, A. D., Wolfire, M., & Leroy, A. K. 2013, *ARA&A*, 51, 207
- Bond, H. E., Bedin, L. R., Bonanos, A. Z., Humphreys, R. M., Monard, L. A. G. B., Prieto, J. L., & Walter, F. M. 2009, *Astrophysical Journal Letters*, 695, L154
- Boyer, M. L., et al. 2015, *ApJS*, 216, 10
- Cardelli, J. A., Clayton, G. C., & Mathis, J. S. 1989, *ApJ*, 345, 245
- Chapman, N. L., Mundy, L. G., Lai, S.-P., & Evans, II, N. J. 2009, *ApJ*, 690, 496
- Cody, A. M., et al. 2014, *AJ*, 147, 82
- Cresci, G., Mannucci, F., Della Valle, M., & Maiolino, R. 2007, *A&A*, 462, 927
- Cunningham, N. J., Moeckel, N., & Bally, J. 2009, *ApJ*, 692, 943
- Dale, J. E., & Davies, M. B. 2006, *MNRAS*, 366, 1424
- Davies, M. B., Bate, M. R., Bonnell, I. A., Bailey, V. C., & Tout, C. A. 2006, *MNRAS*, 370, 2038
- Ennis, D., Beckwith, S., Gatley, I., Matthews, K., Becklin, E. E., Elias, J., Neugebauer, G., & Willner, S. P. 1977, *ApJ*, 214, 478
- Fazio, G. G., et al. 2004, *ApJS*, 154, 10
- Fox, O., Filippenko, A., Skrutskie, M., Arendt, R., Cenko, B., & Van Dyk, S. 2012, A Search for the Missing Supernovae in Ultraluminous, Star Forming Galaxies, Spitzer Proposal
- Fox, O. D., Filippenko, A. V., Skrutskie, M. F., Silverman, J. M., Ganeshalingam, M., Cenko, S. B., & Clubb, K. I. 2013, *AJ*, 146, 2
- Fox, O. D., et al. 2011, *ApJ*, 741, 7
- . 2016, *Astrophysical Journal Letters*, 816, L13
- Gallagher, J. S., & Ney, E. P. 1976, *Astrophysical Journal Letters*, 204, L35
- Gehrz, R. D., Hackwell, J. A., Grasdalen, G. I., Ney, E. P., Neugebauer, G., & Sellgren, K. 1980, *ApJ*, 239, 570
- Gehrz, R. D., Jones, T. J., Matthews, K., Neugebauer, G., Woodward, C. E., Hayward, T. L., & Greenhouse, M. A. 1995, *AJ*, 110, 325
- Gehrz, R. D., et al. 2007, *Review of Scientific Instruments*, 78, 011302
- Gies, D. R., & Bolton, C. T. 1986, *ApJS*, 61, 419
- Goddi, C., Humphreys, E. M. L., Greenhill, L. J., Chandler, C. J., & Matthews, L. D. 2011, *ApJ*, 728, 15
- Gómez, L., Rodríguez, L. F., Loinard, L., Lizano, S., Allen, C., Poveda, A., & Menten, K. M. 2008, *ApJ*, 685, 333
- Gualandris, A., Portegies Zwart, S., & Eggleton, P. P. 2004, *MNRAS*, 350, 615
- Hirota, A., et al. 2014, *PASJ*, 66, 46
- Hoogerwerf, R., de Bruijne, J. H. J., & de Zeeuw, P. T. 2000, *Astrophysical Journal Letters*, 544, L133
- . 2001, *A&A*, 365, 49
- Hosokawa, T., & Omukai, K. 2009, *ApJ*, 691, 823
- Ivanova, N., Justham, S., Avendano Nandez, J. L., & Lombardi, J. C. 2013, *Science*, 339, 433
- Jacobs, B. A., Rizzi, L., Tully, R. B., Shaya, E. J., Makarov, D. I., & Makarova, L. 2009, *AJ*, 138, 332
- Jang, I. S., Lim, S., Park, H. S., & Lee, M. G. 2012, *Astrophysical Journal Letters*, 751, L19
- Jencson, J. E., et al. 2015, *The Astronomer's Telegram*, 7929
- . 2016a, *The Astronomer's Telegram*, 8688
- . 2016b, *The Astronomer's Telegram*, 8940
- Johansson, J., et al. 2014, *ArXiv e-prints*
- Kaifu, N., et al. 2000, *PASJ*, 52, 1
- Kankare, E., et al. 2008, *Astrophysical Journal Letters*, 689, L97
- . 2012, *Astrophysical Journal Letters*, 744, L19
- Kashi, A., & Soker, N. 2016, *Research in Astronomy and Astrophysics*, 16, 014
- Kasliwal, M., et al. 2013, SPIRITS: SPitzer InfraRed Intensive Transients Survey, Spitzer Proposal
- . 2014a, SPIRITS: SPitzer InfraRed Intensive Transients Survey, Spitzer Proposal
- Kasliwal, M., Lau, R., Cao, Y., et al. 2016, Spitzer Proposal, 13053
- Kasliwal, M. M. 2012, *Publications of the Astronomical Society of Australia*, 29, 482
- Kasliwal, M. M., Lovelace, R. V. E., & Houck, J. R. 2005, *ApJ*, 630, 875
- Kasliwal, M. M., et al. 2014b, *The Astronomer's Telegram*, 6644
- Kochanek, C. S. 2011, *ApJ*, 741, 37
- Kochanek, C. S., Adams, S. M., & Belczynski, K. 2014, *MNRAS*, 443, 1319
- Kozłowski, S., et al. 2010, *ApJ*, 722, 1624
- Kwan, J., & Scoville, N. 1976, *Astrophysical Journal Letters*, 210, L39
- Lau, R. M., et al. 2016, *ArXiv e-prints*
- Lovegrove, E., & Woosley, S. E. 2013, *ApJ*, 769, 109
- Low, F. J., Rieke, G. H., & Gehrz, R. D. 2007, *ARA&A*, 45, 43
- Mattila, S., et al. 2007, *Astrophysical Journal Letters*, 659, L9

Table 1. SPRITES: Co-ordinates and Host Galaxies

Name	RA (J2000)	DEC (J2000)	Host Galaxy	Distance Modulus
SPIRITS 14qk	09 ^h 55 ^m 28.72 ^s	+69°39′58.6″	MESSIER 82	27.73 (Jacobs et al. 2009)
SPIRITS 14afv	12 ^h 50 ^m 49.56 ^s	+41°05′52.7″	MESSIER 94	28.31 (Tully et al. 2013)
SPIRITS 14agd	13 ^h 05 ^m 30.87 ^s	−49°26′50.8″	NGC 4945	27.90 (Mould & Sakai 2008)
SPIRITS 14ajc	13 ^h 36 ^m 52.95 ^s	−29°52′16.1″	MESSIER 83	28.41 (Radburn-Smith et al. 2011)
SPIRITS 14ajd	13 ^h 37 ^m 05.02 ^s	−29°48′56.2″	MESSIER 83	28.41 (Radburn-Smith et al. 2011)
SPIRITS 14aje	14 ^h 02 ^m 55.51 ^s	+54°23′18.5″	MESSIER 101	29.34 (Tikhonov et al. 2015)
SPIRITS 14ajp	13 ^h 37 ^m 12.71 ^s	−29°49′14.9″	MESSIER 83	28.41 (Radburn-Smith et al. 2011)
SPIRITS 14ajr	13 ^h 36 ^m 54.81 ^s	−29°52′33.7″	MESSIER 83	28.41 (Radburn-Smith et al. 2011)
SPIRITS 14ave	03 ^h 47 ^m 03.17 ^s	+68°09′05.3″	IC 342	27.58 (Wu et al. 2014)
SPIRITS 14axa	09 ^h 56 ^m 01.52 ^s	+69°03′12.5″	MESSIER 81	27.80 (Jang et al. 2012)
SPIRITS 14axb	07 ^h 36 ^m 34.70 ^s	+65°39′22.4″	NGC 2403	27.51 (Radburn-Smith et al. 2011)
SPIRITS 14bay	12 ^h 56 ^m 43.25 ^s	+21°42′25.7″	MESSIER 64	29.37 (Tully et al. 2013)
SPIRITS 14bgq	13 ^h 39 ^m 50.99 ^s	−31°38′46.0″	NGC 5253	27.76 (Mould & Sakai 2008)
SPIRITS 14bsb	01 ^h 35 ^m 06.72 ^s	−41°26′13.5″	NGC 625	28.12 (Jacobs et al. 2009)

Table 2. Light Curve Properties of SPRITES

Name	Peak Time [3.6] MJD	Peak Mag [3.6] Mag	Peak Time [4.5] MJD	Peak Mag [4.5] Mag	Color Peak Time [3.6]-[4.5] MJD	Color Peak Mag [3.6]-[4.5] Mag	Progenitor limit [3.6] Mag	Progenitor limit [4.5] Mag	Lifespan [3.6] yr	Evolution [3.6] mag yr ^{−1}	Lifespan [4.5] yr	Evolution [4.5] mag yr ^{−1}	Speed
SPIRITS 14ave	57007.4	−11.2	57007.4	−11.8	57182.2	0.3	−10.6	−10.8	1.0	0.1	1.0	0.5	Slow
SPIRITS 14afv	56722.7	−11.4	56754.9	−12.1	57250.7	1.2	−10.6	−10.9	1.4	0.9	2.1	0.5	Fast
SPIRITS 14ajp	56787.2	−11.3	55290.7	−11.9	56915.5	0.7	−10.0	−10.3	5.6	0.2	4.4	<0.1	Slow
SPIRITS 14axb	56827.4	−11.3	56827.4	−11.9	56827.4	0.6	−7.90	−9.37	0.1	−32.2	0.4	−6.2	Fast
SPIRITS 14bay	56889.8	−11.4	56889.8	−12.6	56889.8	1.2	−11.4	−11.5	Fast
SPIRITS 14ajr	56915.5	−11.3	56787.2	−12.2	56915.5	0.8	−11.1	−11.5	4.4	−0.1	5.0	0.1	Slow
SPIRITS 14axa	56821.9	−11.1	56821.9	−11.6	56821.9	0.5	−9.19	−9.56	Fast
SPIRITS 14agd	56764.5	−11.5	56544.9	−13.6	56787.1	0.9	−11.3	−11.7	1.1	−0.1	1.6	1.5	Fast
SPIRITS 14bgq	55424.4	−10.8	55424.4	−11.6	57312.2	0.8	5.6	<0.1	5.6	<0.1	Slow
SPIRITS 14qk	56831.7	−10.9	54430.7	−11.2	56846.3	0.4	−10.6	−10.7	0.7	0.9	7.1	<0.1	Fast
SPIRITS 14ajc	56765.1	−11.3	56765.1	−12.2	57161.2	0.5	−10.6	−11.4	5.1	<0.1	5.1	0.1	Slow
SPIRITS 14aje	56742.8	−11.9	56742.8	−13.7	56771.8	1.6	−10.5	−11.6	0.4	2.4	0.1	7.3	Fast
SPIRITS 14ajd	55290.7	−11.2	55290.7	−12.2	56915.5	1.0	−10.3	−10.9	4.4	0.1	5.1	0.3	Slow
SPIRITS 14bsb	57078.5	−12.5	57085.0	−13.3	57446.6	1.5	1.9	0.6	1.9	<0.1	Fast

Table 3. SPIRITS 14ajc Emission Lines

Transition	Wavelength	Flux	FWHM	Relative Velocity	Flux Ratio (Observed)	Flux Ratio if 1000K	Flux Ratio if 2000K	Flux Ratio if 3000K	Flux Ratio if 4000K
1-0 S(0)	22275.1	11.43	8.96	28	0.28	0.27	0.21	0.19	0.19
1-0 S(1)	21258.9	40.13	6.74	65	1.00	1.00	1.00	1.00	1.00
2-1 S(3)	20774.4	8.013	9.74	57	0.20	0.003	0.084	0.27	0.47
1-0 S(2)	20376.4	10.61	6.04	53	0.26	0.27	0.37	0.42	0.44
1-0 S(3)	19613.6	25.67	6.71	63	0.64	0.51	1.02	1.29	1.45

McLean, I. S., et al. 2012, in Proc. SPIE, Vol. 8446, Ground-based and Airborne Instrumentation for Astronomy IV, 84460J

Menten, K. M., Reid, M. J., Forbrich, J., & Brunthaler, A. 2007, A&A, 474, 515

Milligan, S., Cranton, B. W., & Skrutskie, M. F. 1996, in Proc. SPIE, Vol. 2863, Current Developments in Optical Design and Engineering VI, ed. R. E. Fischer & W. J. Smith, 2–13

Moeckel, N., & Bally, J. 2006, ApJ, 653, 437

—. 2007a, Astrophysical Journal Letters, 661, L183

—. 2007b, ApJ, 656, 275

Mould, J., & Sakai, S. 2008, Astrophysical Journal Letters, 686, L75

Ney, E. P., & Hatfield, B. F. 1978, Astrophysical Journal Letters, 219, L111

Nicholls, C. P., et al. 2013, MNRAS, 431, L33

O’Connell, B., Smith, M. D., Froebrich, D., Davis, C. J., & Eisloffel, J. 2005, A&A, 431, 223

Pejcha, O., Metzger, B. D., & Tomida, K. 2016, MNRAS, 455, 4351

Piro, A. L. 2013, Astrophysical Journal Letters, 768, L14

Prieto, J. L., Kistler, M. D., Thompson, T. A., et al. 2008, Astrophysical Journal Letters, 681, L9

Radburn-Smith, D. J., et al. 2011, ApJS, 195, 18

Rebull, L. M., et al. 2014, AJ, 148, 92

Table 4. Follow-up Photometry

Name	Observation Date	Telescope	Instrument	Filter	Photometry
SPIRITS 14qk	2014 stack (N=74)	P48	iPTF	R	>23.5
SPIRITS 14afv	2014 stack (N=117)	P48	iPTF	R	>20.1
	2014-06-19	MLOF	2MASS	J	>17.4
	2014-06-19	MLOF	2MASS	H	>17.3
	2014-06-19	MLOF	2MASS	Ks	>16.2
SPIRITS 14agd	2014 stack (N=16)	Swope	CCD	g	>21.7
	2014 stack (N=16)	Swope	CCD	r	>21.2
	2014 stack (N=16)	Swope	CCD	i	>21.0
SPIRITS 14ajc	2014-04-20	Swope	CCD	g	>20.0
	2014-04-20	Swope	CCD	r	>20.0
	2014-04-20	Swope	CCD	i	>19.8
	2014-05-18	du Pont	Retrocam	J	>19.8
	2014-05-18	du Pont	Retrocam	H	>18.7
	2014-07-02	Keck	DEIMOS	I	>23.5
	2014-06-07	Keck	MOSFIRE	Ks	>18.7
	2012-09-03	HST	WFC3	H	> 22.0
	2012-07-22	HST	WFC3	I	> 25.5
SPIRITS 14ajd	2014-04-20	Swope	CCD	g	>20.0
	2014-04-20	Swope	CCD	r	>20.0
	2014-04-20	Swope	CCD	i	>19.8
	2014-06-07	Keck	MOSFIRE	Ks	>19.6
	2014-05-24	MLOF	2MASS	J	>17.3
	2014-05-24	MLOF	2MASS	H	>16.5
	2014-05-24	MLOF	2MASS	Ks	>16.4
SPIRITS 14aje	2014 stack (N=157)	P48	iPTF	R	>23.9
	2014-05-01	MLOF	2MASS	J	>18.3
	2014-05-01	MLOF	2MASS	H	>16.8
	2014-05-01	MLOF	2MASS	Ks	>16.4
	2014-07-02	Keck	DEIMOS	I	>24.3
	2014-06-07	Keck	MOSFIRE	Ks	>19.4
	2014-06-07	Keck	MOSFIRE	J	>20.5
	2014-09-23	HST	WFC3	I	>26.5
	2014-09-23	HST	WFC3	J	>25.0
	2014-09-23	HST	WFC3	H	>22.5
SPIRITS 14ajp	2014-04-20	Swope	CCD	g	>20.0
	2014-04-20	Swope	CCD	r	>20.0
	2014-04-20	Swope	CCD	i	>19.8
	2014-06-07	Keck	MOSFIRE	Ks	>19.2
SPIRITS 14ajr	2014-04-20	Swope	CCD	g	>20.0
	2014-04-20	Swope	CCD	r	>20.0
	2014-04-20	Swope	CCD	i	>19.8
	2014-06-07	Keck	MOSFIRE	Ks	>19.2
	2014-05-24	MLOF	2MASS	J	>17.3
	2014-05-24	MLOF	2MASS	H	>16.5
	2014-05-24	MLOF	2MASS	Ks	>16.4
SPIRITS 14ave	2014-09-23	LCOGT-1m	SBIG	i	>20.0
	2014-10-26	LCOGT-1m	SBIG	i	>20.3
SPIRITS 14axa	2014 stack (N=117)	P48	iPTF	R	>23.15
	2014-09-26	HST	WFC3	H	>22.5
SPIRITS 14axb	2014 stack (N=18)	P48	iPTF	R	>22.5
	2014-05-01	MLOF	2MASS	J	>14.2
	2014-05-01	MLOF	2MASS	H	>14.0
	2014-05-01	MLOF	2MASS	Ks	>13.3
SPIRITS 14bay	2014 stack (N=66)	P48	iPTF	R	>23.3
SPIRITS 14bgq	2014 stack (N=12)	Swope	CCD	g	>21.9
	2014 stack (N=12)	Swope	CCD	r	>20.9
	2014 stack (N=10)	Swope	CCD	i	>21.0
	2014-04-30	MLOF	2MASS	J	>16.9
	2014-04-30	MLOF	2MASS	H	>15.6
	2014-04-30	MLOF	2MASS	Ks	>15.7
SPIRITS 14bsb	2014 stack (N=13)	Swope	CCD	g	>22.9
	2014 stack (N=13)	Swope	CCD	r	>22.6
	2014 stack (N=13)	Swope	CCD	i	>22.1

NOTE—This Table is published in its entirety (including individual epochal observations) in the machine-readable format. Upper limits are 5σ .

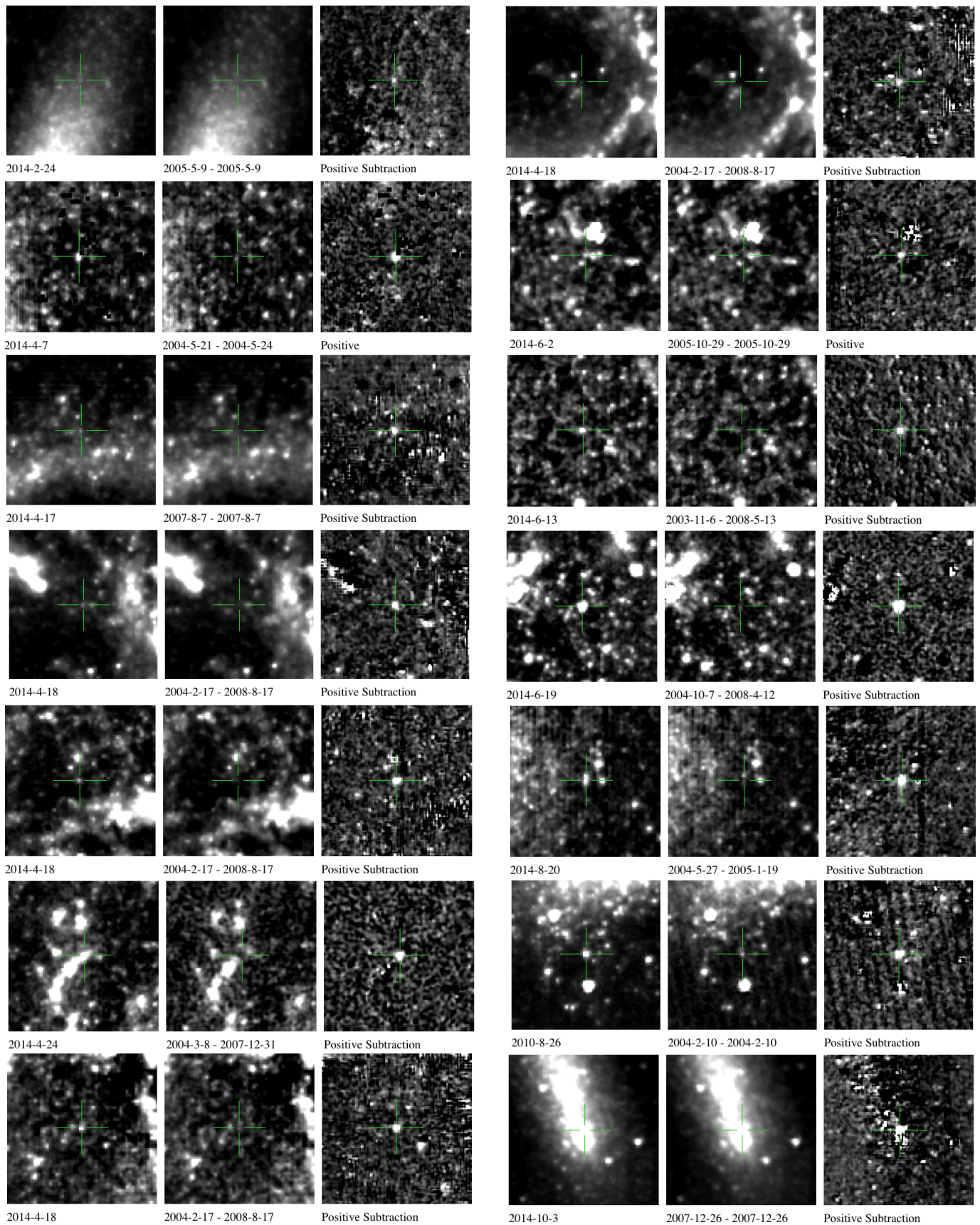


Figure 1. Thumbnails of discovery, reference and subtraction images. The left column is SPIRITS 14qk, 14afv, 14agd, 14ajc, 14ajd 14aje and 14ajp. The right column is SPIRITS 14ajr, 14ave, 14axa, 14axb, 14bay, 14bgq and 14bsb.

Table 5. Spitzer Photometry of all SPRITEs

Name	Observation Date	Filter	Magnitude
SPIRITS 14aje	53072.09	[3.6]	>19.25
SPIRITS 14aje	53072.49	[3.6]	>17.93
SPIRITS 14aje	56048.39	[3.6]	>18.59
SPIRITS 14aje	56742.84	[3.6]	17.25 ± 0.01
SPIRITS 14aje	56771.83	[3.6]	17.79 ± 0.02
SPIRITS 14aje	56771.83	[3.6]	17.74 ± 0.01
SPIRITS 14aje	56902.01	[3.6]	18.29 ± 0.02
SPIRITS 14aje	57136.69	[3.6]	>18.68
SPIRITS 14aje	57144.06	[3.6]	>18.79
SPIRITS 14aje	57150.17	[3.6]	>18.77
SPIRITS 14aje	57163.72	[3.6]	>18.79
SPIRITS 14aje	57163.72	[3.6]	>18.44
SPIRITS 14aje	57191.83	[3.6]	>18.43
SPIRITS 14aje	57191.83	[3.6]	>18.20
SPIRITS 14aje	57220.80	[3.6]	>18.66
SPIRITS 14aje	57247.82	[3.6]	>18.87
SPIRITS 14aje	57486.85	[3.6]	>18.27
SPIRITS 14aje	56742.84	[4.5]	15.52 ± 0.01
SPIRITS 14aje	56771.83	[4.5]	16.10 ± 0.01
SPIRITS 14aje	56771.83	[4.5]	16.12 ± 0.01
SPIRITS 14aje	56902.01	[4.5]	>17.85
SPIRITS 14aje	57136.69	[4.5]	>18.06
SPIRITS 14aje	57144.06	[4.5]	>17.98
SPIRITS 14aje	57150.17	[4.5]	>18.05
SPIRITS 14aje	57163.72	[4.5]	>18.01
SPIRITS 14aje	57163.72	[4.5]	>17.83
SPIRITS 14aje	57191.83	[4.5]	>17.94
SPIRITS 14aje	57191.83	[4.5]	>17.73
SPIRITS 14aje	57220.80	[4.5]	>17.91
SPIRITS 14aje	57247.82	[4.5]	>18.06
SPIRITS 14aje	57486.85	[4.5]	>17.85
SPIRITS 14axb	53286.42	[3.6]	>19.53
SPIRITS 14axb	55146.68	[3.6]	>19.28
SPIRITS 14axb	55168.73	[3.6]	>19.31
SPIRITS 14axb	55181.97	[3.6]	>19.20
SPIRITS 14axb	55302.72	[3.6]	>19.39
SPIRITS 14axb	55339.45	[3.6]	>19.20
SPIRITS 14axb	56671.43	[3.6]	>19.04
SPIRITS 14axb	56795.32	[3.6]	19.07 ± 0.03
SPIRITS 14axb	56827.40	[3.6]	16.24 ± 0.01
SPIRITS 14axb	57174.60	[3.6]	>19.16
SPIRITS 14axb	57180.81	[3.6]	>18.86
SPIRITS 14axb	57201.79	[3.6]	>18.82
SPIRITS 14axb	57388.85	[3.6]	>19.04
SPIRITS 14axb	57395.55	[3.6]	>19.13
SPIRITS 14axb	57409.70	[3.6]	>19.23
SPIRITS 14axb	56671.43	[4.5]	18.30 ± 0.03
SPIRITS 14axb	56795.32	[4.5]	18.30 ± 0.03
SPIRITS 14axb	56827.40	[4.5]	15.64 ± 0.01
SPIRITS 14axb	57174.60	[4.5]	>18.48
SPIRITS 14axb	57180.81	[4.5]	>18.61
SPIRITS 14axb	57201.79	[4.5]	>18.55
SPIRITS 14axb	57388.85	[4.5]	>18.54
SPIRITS 14axb	57395.55	[4.5]	>18.55
SPIRITS 14axb	57409.70	[4.5]	>18.48

NOTE—This Table is published in its entirety (including all SPRITEs) in the machine-readable format. A portion is shown here for guidance regarding its form and content.

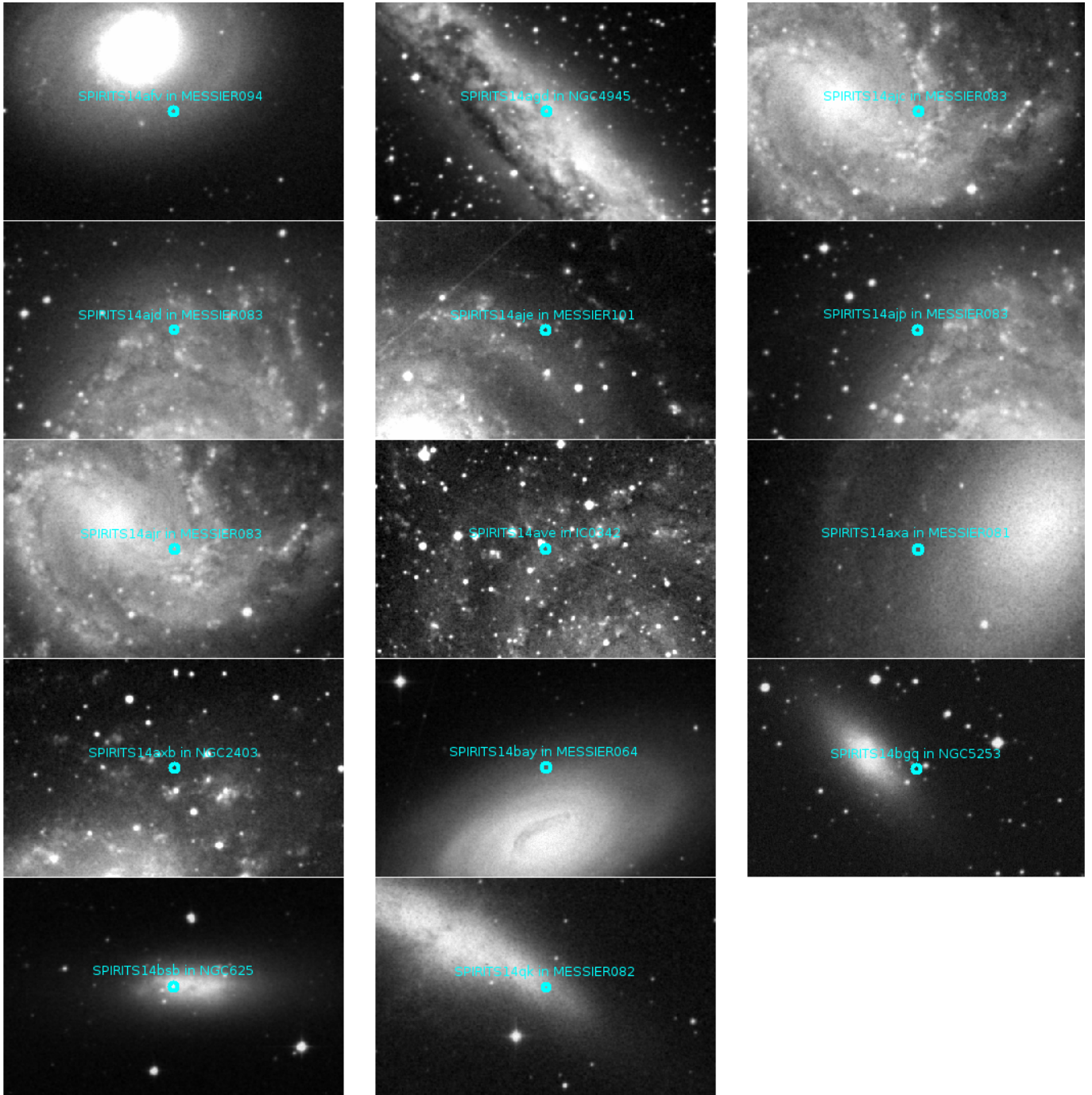


Figure 2. Collage of host galaxies of 14 IR transients discovered by SPIRITS. Background images are $6.9' \times 4.6'$, centered on the SPRITE location, and taken from the Digitized Sky Survey.

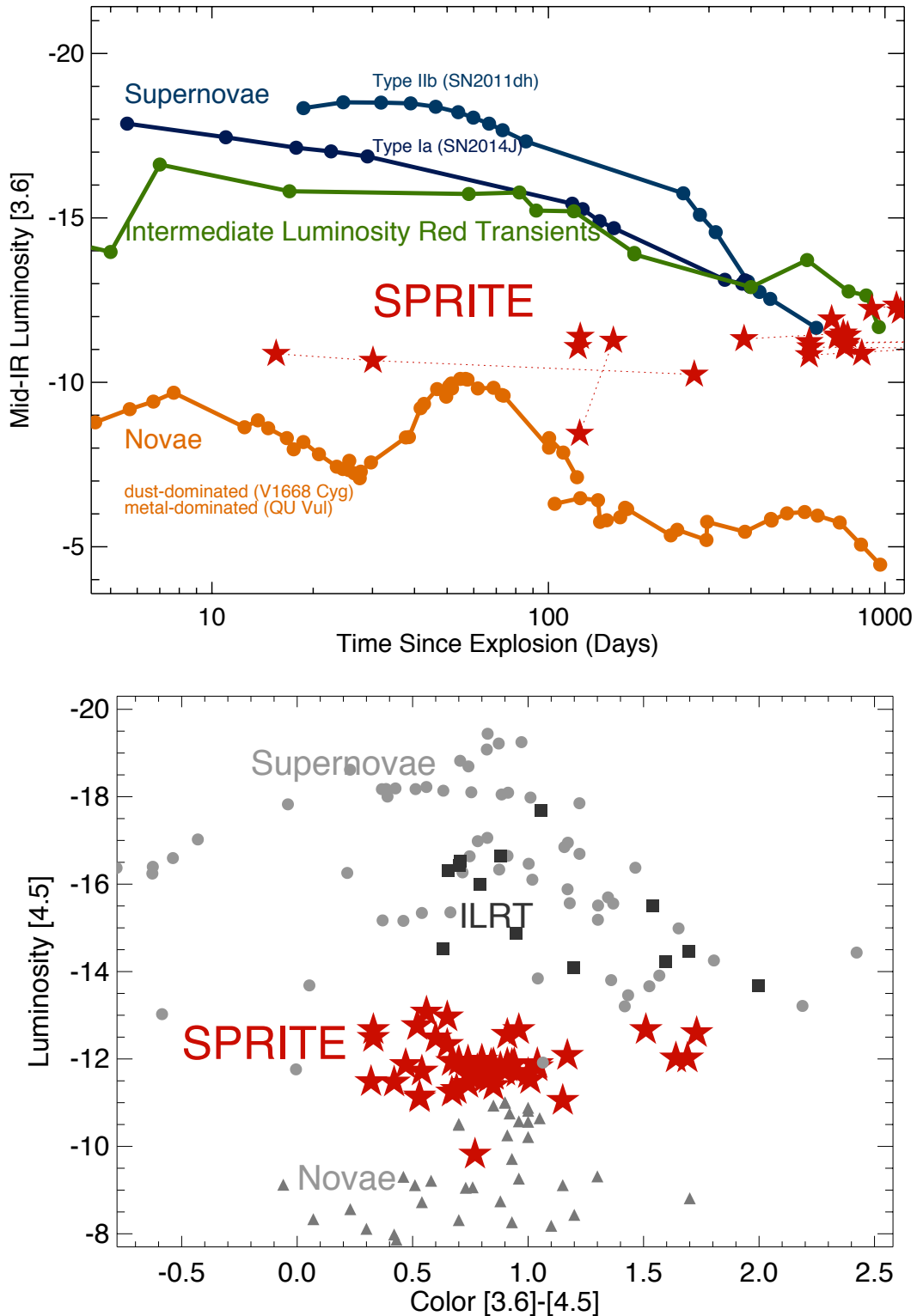


Figure 3. *Top:* Light curves of SPRITEs (red stars) are in the mid-IR luminosity gap between novae (orange) and supernovae (blue). Note that the assumed explosion time for SPRITEs is the last non-detection in archival data (and hence, the phase is a conservative upper limit). *Bottom:* A luminosity-color rendition of the phase space of IR explosions illustrating the unique location of SPRITEs (corresponding effective temperatures are between 350 K and 1000 K). The comparison set includes all detections of all known supernovae hosted by SPIRITS galaxies (Tinyant et al. 2016; Johansson et al. 2014) and two Galactic classical novae (Gehrz et al. 1995, 1980). Detections at all epochs in the light curve for each transient is shown.

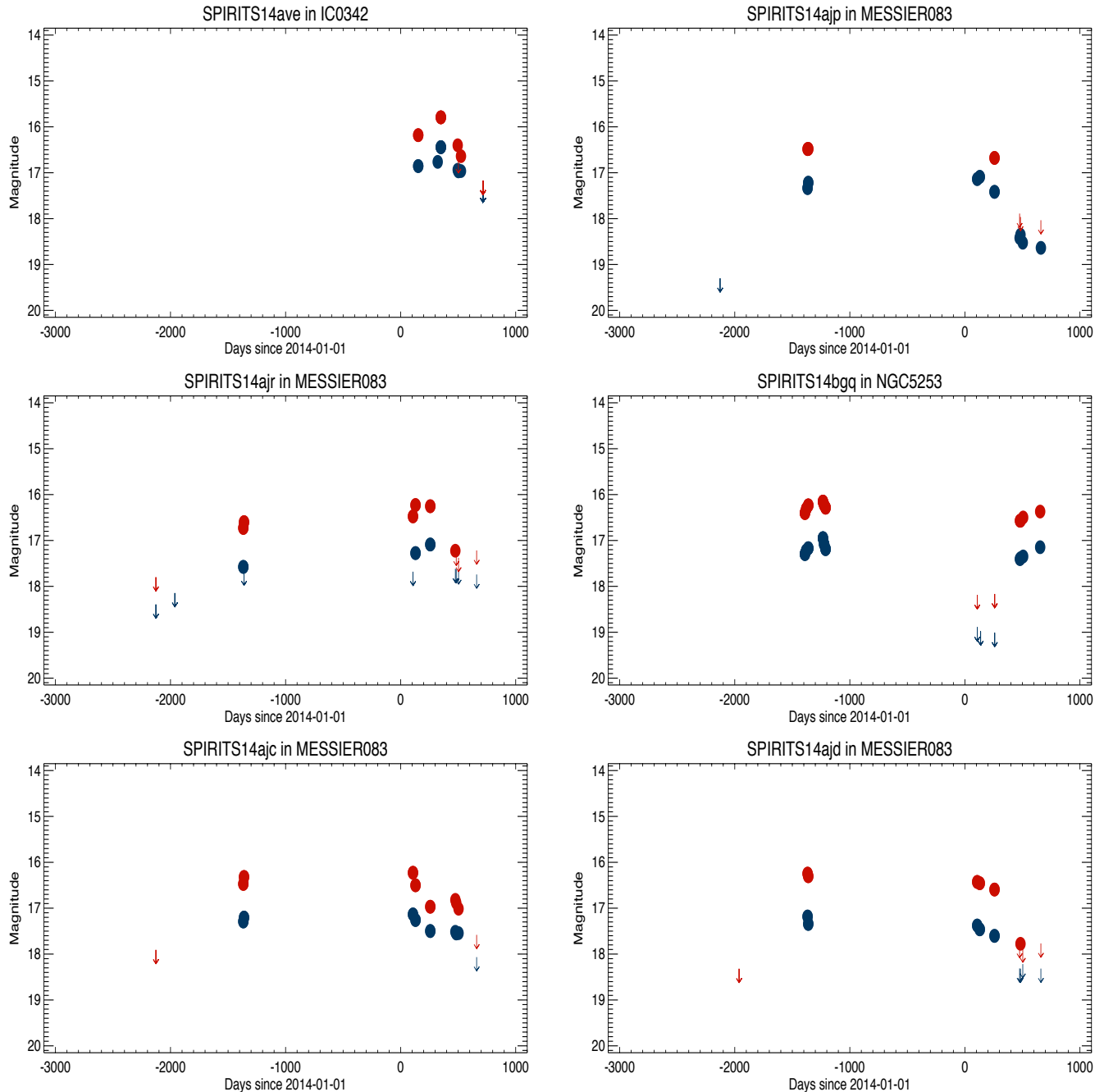


Figure 4. IR light curves of relatively slow evolving SPRITES.

Skrutskie, M. F., et al. 2006, *AJ*, 131, 1163
 Smith, N., et al. 2016, *MNRAS*, 458, 950
 Snell, R. L., Scoville, N. Z., Sanders, D. B., & Erickson, N. R. 1984, *ApJ*, 284, 176
 Soker, N., & Tylenda, R. 2006, *MNRAS*, 373, 733
 Sullivan, P. W., Croll, B., & Simcoe, R. A. 2014, in *Proc. SPIE*, Vol. 9154, High Energy, Optical, and Infrared Detectors for Astronomy VI, 91541F
 Testi, L., Tan, J. C., & Palla, F. 2010, *A&A*, 522, A44
 Thompson, T. A., Prieto, J. L., Stanek, K. Z., Kistler, M. D., Beacom, J. F., & Kochanek, C. S. 2009, *ApJ*, 705, 1364
 Thornton, D., et al. 2013, *Science*, 341, 53

Tikhonov, N. A., Lebedev, V. S., & Galazutdinova, O. A. 2015, *Astronomy Letters*, 41, 239
 Tinyanont, S., et al. 2016, *ArXiv e-prints*
 Tully, R. B., et al. 2013, *AJ*, 146, 86
 Tylenda, R., et al. 2011, *A&A*, 528, A114
 Werner, M. W., et al. 2004, *ApJS*, 154, 1
 Wu, P.-F., Tully, R. B., Rizzi, L., Dolphin, A. E., Jacobs, B. A., & Karachentsev, I. D. 2014, *AJ*, 148, 7
 Zapata, L. A., Schmid-Burgk, J., Ho, P. T. P., Rodríguez, L. F., & Menten, K. M. 2009, *Astrophysical Journal Letters*, 704, L45

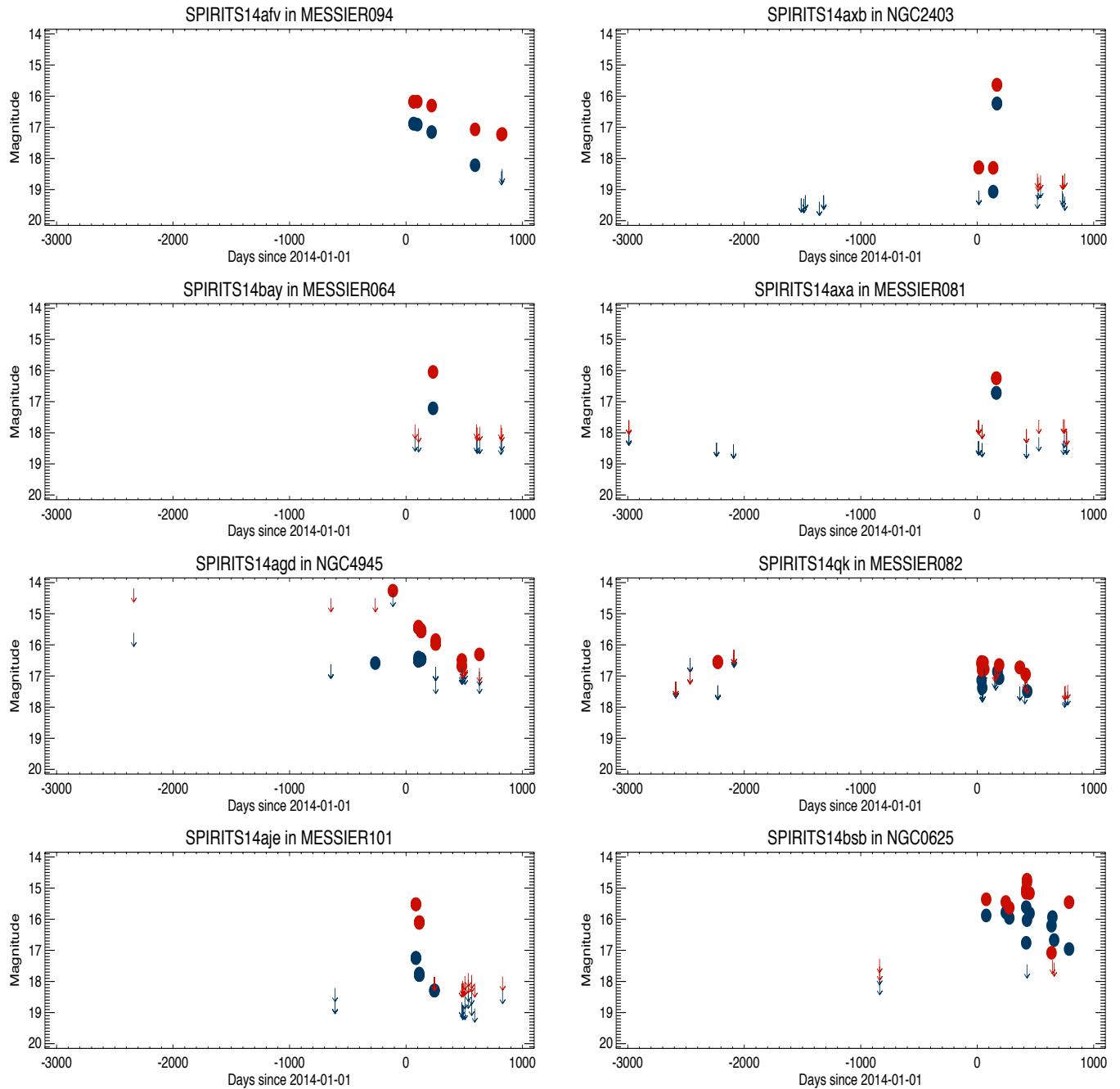


Figure 5. IR light curves of relatively fast evolving SPRITEs.

Zapata, L. A., Schmid-Burgk, J., Pérez-Goytia, N., Ho, P. T. P., Rodríguez, L. F., Loinard, L., & Cruz-González, I. 2013, *Astrophysical Journal Letters*, 765, L29

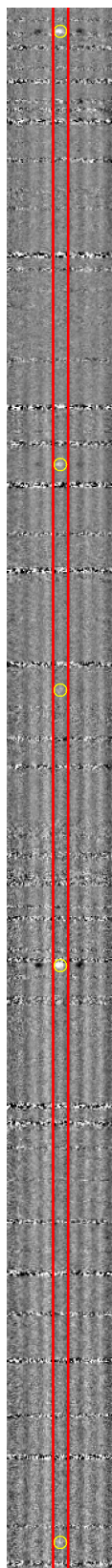


Figure 6. Calibrated and rectified 2-d spectrum of SPIRITS 14ajc (y-axis is the spectral and x-axis is the spatial dimension). Note the five lines of excited molecular hydrogen (yellow circles) and lack of continuum at the trace position of SPIRITS 14jac (red lines). The spectrum spans 19565\AA to 22320\AA in the K-band. The horizontal striped lines are sky line residuals.

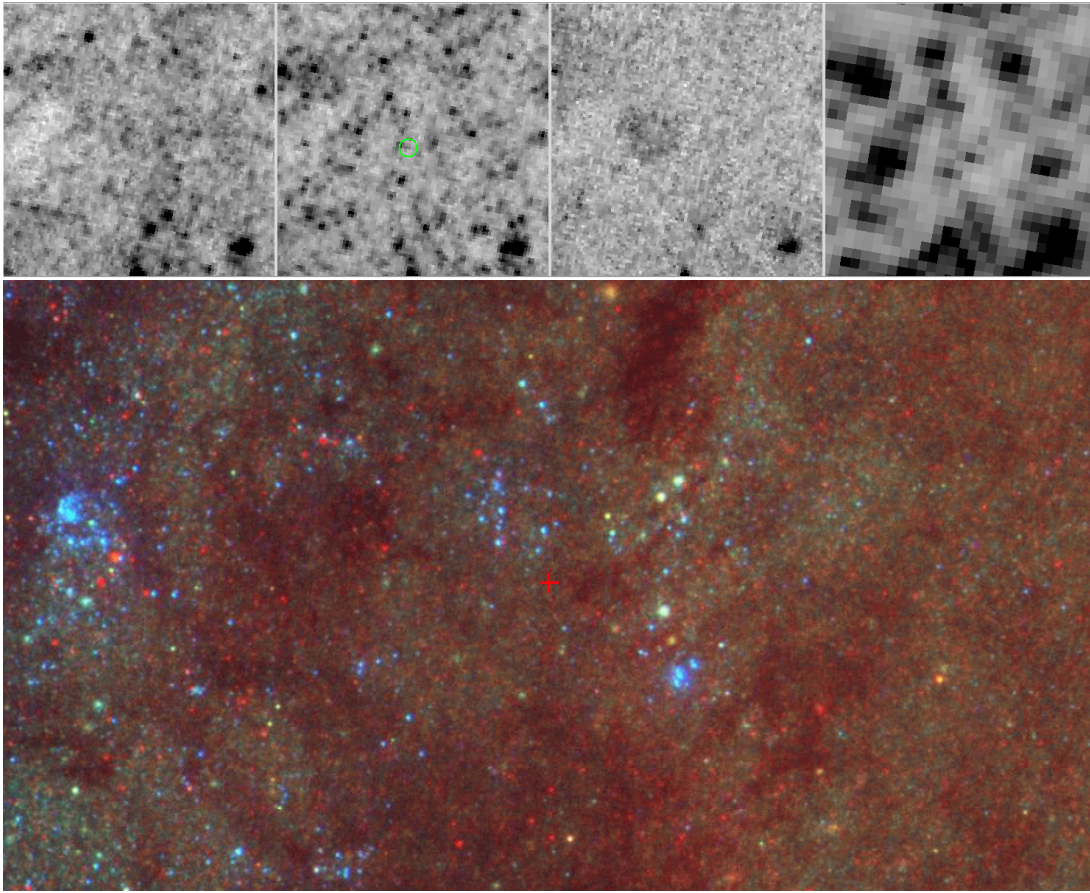


Figure 7. *Top:* *HST* WFC3 images of the site of SPIRITS 14ajc in M83, taken in 2012 while the event was underway. Frames are $3''.6$ high, and have north at the top and east on the left. From left to right the frames are in V (F547M), I (F814W), $H\alpha+[N II]$ (F657N), and H (F160W). The green circle in the F814W image marks the position of the transient, with a radius corresponding to the 3σ positional uncertainty (alignment RMS was $0''.04$). There is a very faint star near the center of the error circle in the F814W image, and a brighter one at the eastern edge, but both are unlikely to be the counterpart of 14ajc. Neither star is detected at H . A faint bubble-like emission nebula lies close to 14ajc in the third frame, but outside the error circle. *Bottom:* Color rendition showing the stellar and ISM environment around SPIRITS 14ajc in M83, made from *HST* images in U , B , and I in the Hubble Legacy Archive. The field is $20''$ high, with north at the top and east on the left. The location of SPIRITS 14ajc is marked with a red cross. The transient lies near several young associations and dark dust lanes, but apparently not within them.